Extratropical Cyclones

Jonathan E. Martin, Department of Atmospheric and Oceanic Sciences, University of Wisconsin-Madison, Madison, WI, United States

© 2024 Elsevier Ltd. All rights are reserved, including those for text and data mining, AI training, and similar technologies.

This is an update of A. Joly, SYNOPTIC METEOROLOGY | Extratropical Cyclones, Editor(s): Gerald R. North, John Pyle, Fuqing Zhang, Encyclopedia of Atmospheric Sciences (Second Edition), Academic Press, 2015, Pages 304–336, ISBN 9780123822253, https://doi.org/10.1016/B978-0-12-382225-3.00128-6.

|---|---|
Introduction	1
Basic Structural and Energetic Characteristics	2
Cyclogenesis: The Development of Extratropical Cyclones	4
The Influence of Diabatic Effects	11
Cyclogenesis from the Potential Vorticity (PV) Perspective	15
A Note on the Global Distribution of Extratropical Cyclones	21
Concluding Statement	21
References	21
Further Reading	22

Key Points

- Extratropical cyclones have life cycles of about a week during which their circulations and associated sensible weather can influence millions of square kilometers.
- Cyclogenesis, the development of a cyclone, is controlled by large-scale dynamical processes endemic to the baroclinic westerly shear of Earth's mid-latitudes. Specifically, differential advection of vorticity in the vertical direction produces low-level convergence and spins up lower tropospheric circulations.
- This basic process is enhanced and made more intense by diabatic feedbacks, most often arising from the release of latent heat associated with the production of precipitation during cyclogenesis.
- Diagnostics of cyclogenesis can be considered in different, but complimentary, frameworks; the basic state variable (omega-centric), and the potential vorticity (PV) frameworks.

Synopsis

Extratropical cyclones are the most recurrent large-scale weather phenomena in the middle latitudes of Earth. They arise from nearly imperceptible disturbances in the baroclinic westerly shear, grow to encompass millions of square kilometers, and exist for about a week. They are responsible for a large fraction of mid-latitude precipitation, especially during the cold season, and their development and progression through a life cycle are the combined product of large-scale dynamical processes and diabatic feedbacks from the latent heat release organized by their characteristic mesoscale frontal structures. In this chapter a broad overview of the structure, dynamics and global distribution of extratropical cyclones is given from an observational, diagnostic perspective.

Introduction

The most recurring large-scale weather phenomena in the middle latitudes of Earth is the extratropical cyclone. As a result of their ubiquity, these storms have been the subject of scientific scrutiny for well over 200 years and surely of general interest for far longer. In fact, pursuit of understanding these important disturbances was arguably the central motivation behind the blossoming of modern meteorology that began just after WW I. In addition, the desire to accurately predict these storms represented one of the first major tests for the newly developed electronic computer just after WW II. Consistent with its being a central organizing feature of interest in mid-latitude meteorology, the extratropical cyclone is the hub of a number of phenomena that are subjects of individual chapters within this section of the Encyclopedia. Consequently, the goal of this chapter is to provide a basic overview of fundamental aspects of these awesome storms. Such aspects include (1) their life cycle characteristics, (2) aspects of their global distribution, (3) and a concise description of their dynamical origins and the processes that contribute to their development and decay from two complimentary perspectives. Throughout this examination the perspective is adopted wherein the extratropical cyclone is the product of development initiated by finite, identifiable disturbances in the flow, not a manifestation of unstable

Reference Collection in Earth Systems and Environmental Sciences   https://doi.org/10.1016/B978-0-323-96026-7.00129-6   1

growth of an infinitesimal perturbation. Though the latter, more mathematical, approach to the problem is laden with insight and supported by a well developed literature, this choice simply reflects a desire to provide the intended overview from an overtly observational perspective. Consistent with this choice, the dynamics of cyclogenesis will be considered from both the quasi-geostrophic (QG) and potential vorticity (PV) diagnostic perspectives. Examination of the post-mature stage will involve consideration of the structural and dynamical nature of the so-called occlusion.

Basic Structural and Energetic Characteristics

The extratropical cyclone is a transient atmospheric disturbance, characteristic of the middle latitudes of Earth, whose organized circulation can influence millions of square kilometers simultaneously. These storms have life cycles of about a week during which they grow from nearly undetectable entities to continental-scale storms before decaying away to nothing and vanishing from the face of Earth. At their cores, extratropical cyclones exhibit local regions of sea-level pressure (SLP) minima and are consequently characterized by cyclonic winds which, in both hemispheres, usher tropical air poleward and polar air equatorward. In fact, of the three main mechanisms at work to alleviate the latitudinal variation in absorbed radiation arising from the sphericity of the Earth and its axial tilt (*latent heat release* and *ocean currents* being the other two), the extratropical cyclone is the most important agent of amelioriation.

   Perhaps the most distinguishing aspect of the extratropical cyclone is its asymmetric thermal structure manifest most obviously in its frontal structure (see Fronts and Frontogenesis). Though research regarding the extratropical cyclone stretches back to the 18th century, it was not until the end of WWI that meteorologists at the University of Bergen developed a theory of the extratropical cyclone life cycle that centered on the evolution of its attendant frontal structure.

   The resulting conceptual model, known at the Norwegian Cyclone Model (NCM, Bjerknes and Solberg 1922) suggested that small scale vortices ocassionally developed along a globe-girdling polar front that separated cold polar air from warm tropical air (Fig. 1A). The circulation associated with these initially small-scale disturbances would serve to locally deform the polar front, forcing tropical air poleward and polar air equatorward (Fig. 1B). Continued intensification of some of these disturbances (for
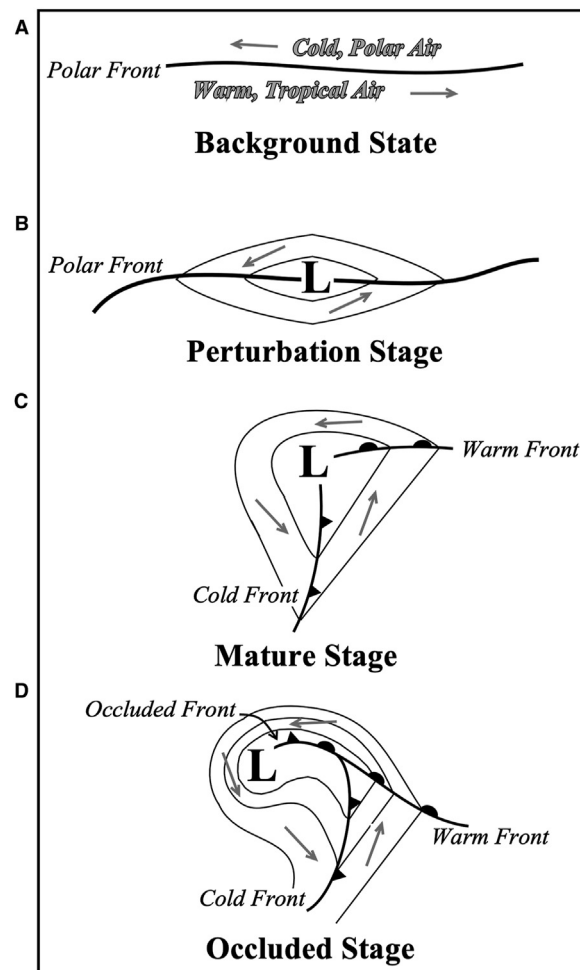
Fig. 1   Evolution of a mid-latitude cyclone according to the Norwegian Cyclone Model. (A) The polar front as a background state. (B) The initial cyclonic perturbation. (C) The mature stage. (D) The occluded stage. The thin solid lines are isobars of sea-level pressure and the arrows are surface wind vectors. Adapted from Martin (2006).
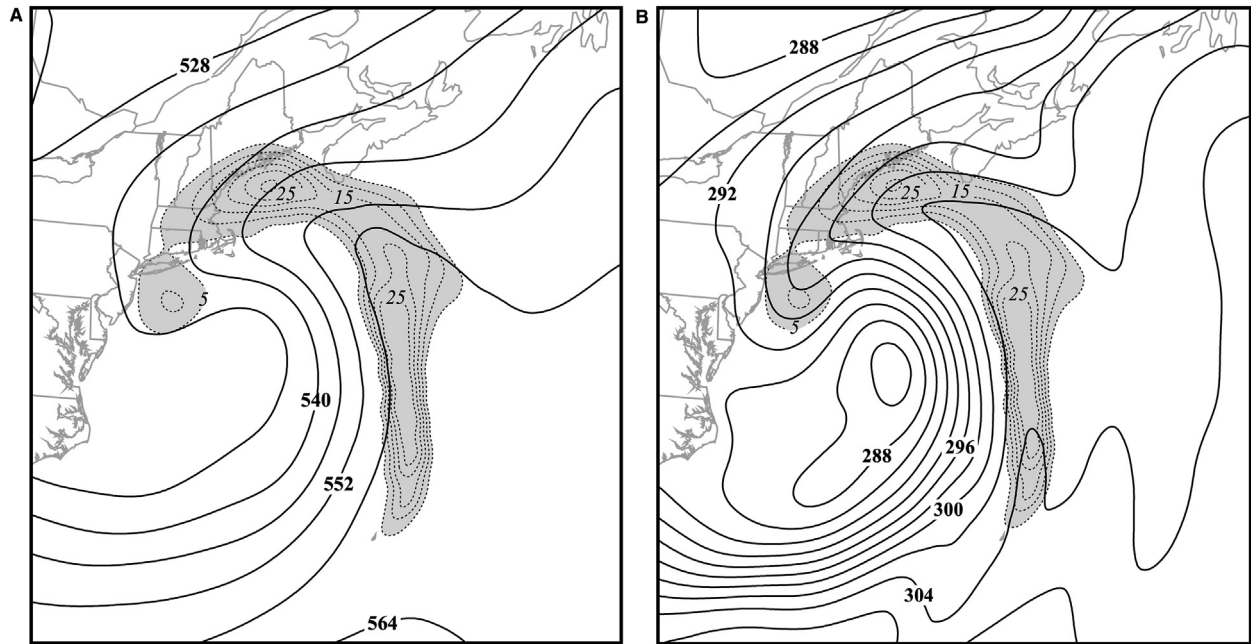
Fig. 2 The characteristic occluded thermal ridge as observed at 0600 UTC April 1, 1997. (A) Solid lines are 1000:500 hPa thickness labeled in dam and contoured every 6 dam. Dashed lines with shading are 700 hPa upward vertical motion labeled in cm s^{-1} and contoured every 5 cm s'. Both variables are from an 18 h forecast of the NCEP Eta model valid at 0600 UTC April 1, 1997. (B) Solid lines are 18 h forecast of 700 hPa θ, valid at 0600 UTC 1 April, labeled in K and contoured every 2 (K) Vertical motion as in **Fig. 2**A. Adapted from Martin (2006).

reasons that were unspecified in the NCM) led to a SLP minimum and local appropriation of the polar front into the familiar warm and cold fronts of the cyclone (**Fig. 1**C). Further intensification of the cyclone was thought to lead to an encroachment of the cold front toward the warm front with the cold front eventually overtaking the warm front while the SLP minimum retreated poleward from the peak of the warm sector in a process known as occlusion (**Fig. 1**D). One of the main results of this process was the production of a wedge of warm air aloft, displaced poleward of the surface warm and (newly created) occluded fronts. As a result of the gradual squeezing of warm air aloft between the two intersecting frontal surfaces, the horizontal thermal structure of a warm occlusion was characterized by a thermal ridge connecting the peak of the warm sector to the geopotential or sea-level pressure minimum (**Fig. 2**). Note that considerable upward vertical motion is also co-located with this thermal ridge. The observation that the cloudiness and precipitation characteristic of the occluded sector of extratropical cyclones often occurs in the vicinity of the thermal ridge led scientists at the Canadian Meteorological Service in the 1950's and 1960's to regard the essential structural feature of a warm occlusion to be the *trough of warm air aloft* (**trowal**) that represented the 3D sloping intersection between the cold and warm frontal baroclinic zones (**Fig. 3**). Defined this way, the trowal represents a refined, 3-D description of the warm occluded structure presented in the NCM. Though high impact sensible weather was still possible at and past the point of occlusion, the intensity of the cyclone as measured by SLP was thought to have reached its peak at this point in the life cycle.

The nearly spherical Earth, tilted at 23.5° to the plane of the ecliptic, is characterized by a pole-to-equator temperature gradient whose intensity varies with the season. Such a temperature gradient is manifest as a baroclinic westerly vertical shear at middle latitudes via the thermal wind balance. Consider a purely zonal mid-latitude flow in thermal wind balance. In such a flow, the middle or upper tropospheric geopotential height lines and isotherms would be everywhere parallel. Now imagine that a wave-like perturbation is introduced into this flow and that the wave moves at precisely the speed of the background flow. In such a case, only the wave's meridional motions would be discernible and they would promote warm air advection downstream of the trough axis and cold air advection upstream of the trough axis as shown in **Fig. 4**. This set of circumstances would eventually produce a wave in the thermal field that would lag the wave in the momentum field by one-quarter wavelength. In order for this perturbation to grow, both the positive and negative zonal temperature anomalies must become larger and the kinetic energy associated with the wave motions must increase.

The pole-to-equator temperature gradient represents a horizontal density contrast conceptually analogous to the simple example shown in **Fig. 5**A. If, by some mechanism, the dense fluid ends up beneath the less dense fluid (as shown in **Fig. 5**B) then the center of mass of the fluid system has been reduced and there has been a conversion of *some* of the initial potential energy into the kinetic energy of the fluid motions involved in the rearrangement. That fraction of the total potential energy that can be converted into kinetic energy is known as the *available potential energy* (APE). Were the wave-like disturbance of **Fig. 4** able to convert the APE of the background zonal baroclinic shear into the kinetic energy of its own motions then the perturbation would grow at the expense of the basic flow. In such a case, the background flow could be deemed unstable to the introduction of the disturbance.
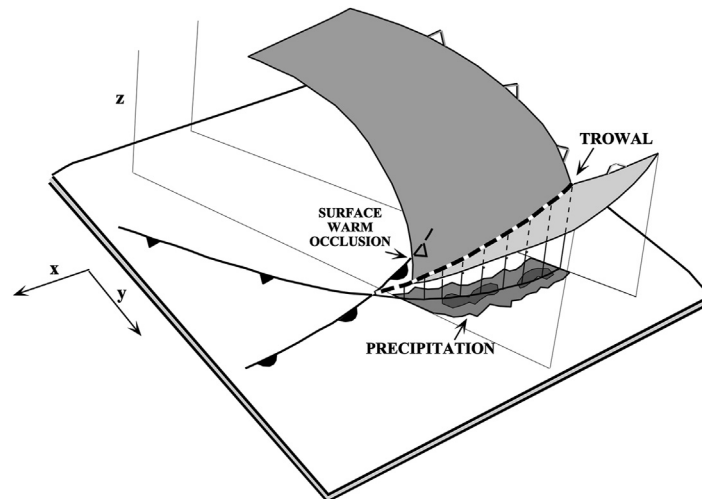
Fig. 3 Schematic of the trowal conceptual model. The dark (light) shaded surface represents the warm edge of the cold (warm) frontal zone. The bold dashed line at the 3-D sloping intersection of those two frontal zones lies at the base of the trough of warm air aloft—the trowal. The schematic precipitation in the occluded quadrant of the cyclone lies closer to the projection of the trowal to the surface than to the position of the surface warm occluded front. Adapted from Martin (2006).

Extratropical cyclones (and anti-cyclones) are wave phenomena. As a result, any regional sea-level pressure analysis, such as the example shown in Fig. 6, will display an alternating sequence of surface high and low pressure disturbances. In order to produce and maintain a surface low (high) pressure center, air must be evacuated from (*packed into*) the atmospheric column above the surface. Air being a continuous fluid, divergence (i.e. mass evacuation) occurs at the top of columns of rising air while convergence (i.e. mass accumulation) occurs at the top of columns of sinking air. Consequently, an alternating sequence of surface highs and lows, each associated with sinking or rising air in their respective columns, characterizes a mid-latitude wave train as shown in Fig. 7A. By virtue of the fact that curvature adds a centrifugal force to the pressure gradient (PGF) and Coriolis (COR) forces that dominate at middle latitudes, the upper tropospheric flow is rendered subgeostrophic at trough axes and supergeostrophic at ridge axes as illustrated in Fig. 8. As a result, upward (*downward*) vertical motions occur downstream of trough (*ridge*) axes at upper tropospheric levels. Thus, regions of low (*high*) geopotential height must be located to the west of the rising (*sinking*) air columns shown in Fig. 7B. Therefore, for developing mid-latitude disturbances (such as extratropical cyclones), the geopotential height axes tilt westward, into the vertical shear, with increasing height.

At the mature stage the extratropical cyclone's low pressure center is located at the peak of the warm sector. The center of the upstream surface anticyclone is close to the center of minimum temperature near sea-level. Since the hypsometric equation relates thickness to column averaged temperature, upper tropospheric geopotential minima (*maxima*) must lie atop relatively cold (*warm*) columns. Thus, as shown in Fig. 7C, the thermal axes of developing mid-latitude waves tilt eastward with increasing height. Since air is rising through the warm column and sinking through the cold column, developing mid-latitude disturbances are characterized by thermally direct vertical circulations which convert the available potential energy of the background baroclinicity, manifest in the westerly vertical shear of the large-scale flow, into the kinetic energy of the disturbances.

The fact that the structure of the extratropical cyclone encourages spontaneous conversion of APE to kinetic energy implies that the background baroclinic shear is, in fact, unstable to certain wave-like perturbations and that extratropical cyclones are a primary manifestation of this instability. A more fully developed version of this baroclinic instability[1] theory suggests that disturbances of the scale of mid-latitude short waves (3000−4500 km in wavelength), in environments characterized by observed values of vertical shear, are those that exhibit the most efficient growth by this mechanism.

Cyclogenesis: The Development of Extratropical Cyclones

The term cyclogenesis is used to describe the set of processes by which a surface cyclone initially develops and subsequently inten-sifies. A common means of assessing intensification is to measure SLP decreases following the cyclone center. Such semi-Lagrangian negative pressure tendencies are invariably attended by increases in the low-level geostrophic vorticity. Thus, cyclogenesis can be viewed as a process of low-level vorticity production which necessitates the presence of divergence and vertical motions. Based upon the continuity equation, the surface pressure tendency at any point is dictated by the total convergence of mass into the vertical

---

[1]Baroclinic instability theory was discovered independently by Charney (1947) and Eady (1949) using approaches to the problem that were significantly different from one another. Charney was also the first to rigorously derive the quasi-geostrophic system of equations.
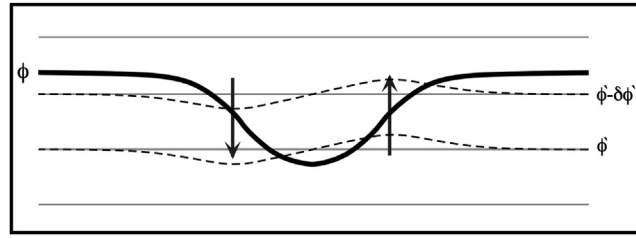
Fig. 4 Effect of introducing a wave in the momentum field into a zonally oriented bundle of column averaged isotherms. Light gray lines are undisturbed thickness isopleths of the mean state. Dashed lines are the disturbed thickness isopleths after the meridional motions of the wave (arrows) have distorted them. Thick black line shows a schematic geopotential height line. Note that the resulting thickness wave is 1/4 wavelength out of phase with the wave in the geopotential height. Adapted from Martin (2006).

column of atmosphere above that point. Consequently, net mass divergence (*convergence*) in the column is responsible for SLP falls (*rises*) at a given location. Since accurately measuring the divergence is a difficult task, consideration of this fundamental relationship relies on a set of approximate equations containing reference to the divergence. The simplest such set of equations are the quasi-geostrophic set which include the quasi-geostrophic vorticity and thermodynamic energy equations given by

$$\frac{\partial \zeta_g}{\partial t} = -\overrightarrow{V_g} \cdot \nabla (\zeta_g + f) + f_o \frac{\partial \omega}{\partial p} \tag{1A}$$

$$\frac{\partial}{\partial t}\left(-\frac{\partial \phi}{\partial p}\right) = -\overrightarrow{V_g} \cdot \nabla \left(-\frac{\partial \phi}{\partial p}\right) + \sigma \omega \tag{1B}$$

respectively. Representing the geopotential tendency as $\chi = \frac{\partial \phi}{\partial t}$, the geostrophic vorticity tendency can be expressed as $\frac{\partial \zeta_g}{\partial t} = \frac{1}{f_o}\nabla^2\chi$ and the above two expressions can be rewritten as

$$\nabla^2\chi = -f_o\,\overrightarrow{V_g} \cdot \nabla \left(\frac{1}{f_o}\nabla^2\phi + f\right) + f_o^2 \frac{\partial \omega}{\partial p} \tag{1B}$$

$$\frac{\partial \chi}{\partial p} = -\overrightarrow{V_g} \cdot \nabla \left(\frac{\partial \phi}{\partial p}\right) - \sigma\omega. \tag{2B}$$

Taking $\frac{f_o^2}{\sigma}\frac{\partial}{\partial p}$ **(2B)** and adding it to **(1B)** eliminates reference to ω (the vertical motion) and yields

$$\left(\nabla^2 + \frac{f_o^2}{\sigma}\frac{\partial^2}{\partial p^2}\right)\chi = -f_o\,\overrightarrow{V_g} \cdot \nabla \left(\frac{1}{f_o}\nabla^2\phi + f\right) - \frac{f_o^2}{\sigma}\frac{\partial}{\partial p}\left(\overrightarrow{V_g} \cdot \nabla \left(\frac{\partial \phi}{\partial p}\right)\right) \tag{3}$$

which is known as the *quasi-geostrophic height tendency equation*. The second order differential operator on the LHS of **(3)** has a simple interpretation; when $\left(\nabla^2 + \frac{f_o^2}{\sigma}\frac{\partial^2}{\partial p^2}\right)\chi$ is less than (*greater than*) zero, then χ itself is greater than (*less than*) zero. The RHS of **(3)** implies
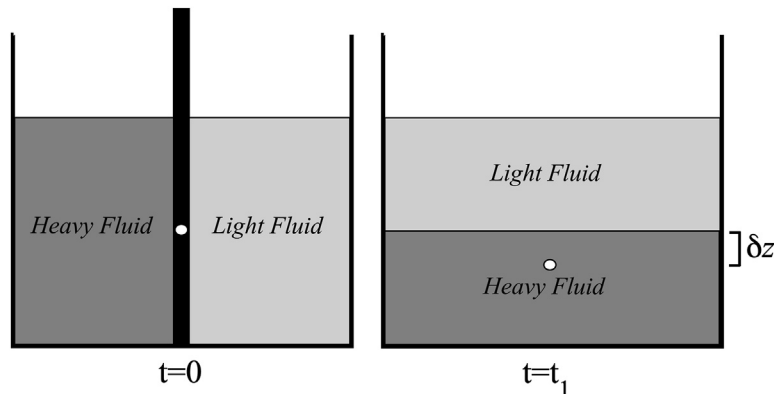
Fig. 5 Fluids of different densities separated horizontally in a container by a dividing wall (thick black line) at t = 0. The white dot represents the height of the center of gravity of the two fluid system. At t = t$_1$ after the divider has been removed, the height of the center of gravity of the fluid system has been lowered by an amount δ_z. Adapted from Martin (2006).
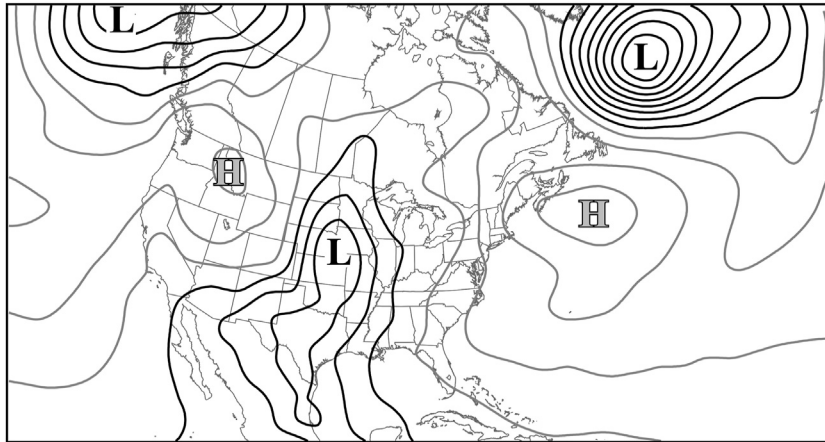
Fig. 6 Sea-level pressure analysis over North America at 1200 UTC April 16, 2004. Solid lines are isobars contoured every 4 hPa with black (gray) lines corresponding to pressures less than (greater than) or equal to 1012 (1016) hPa. "L"s and "H"s identify centers of surface low and high pressure systems, respectively. Adapted from Martin (2006).

that there are two processes that can contribute to local geopotential height changes. The first, $-f_o \overrightarrow{V_g} \cdot \nabla \left(\frac{1}{f_o} \nabla^2 \phi + f \right)$, describes the effect of geostrophic vorticity advection on height falls. Fig. 9 shows a schematic upper tropospheric trough with a cyclonic vorticity maxima at its base. Immediately to the east (*west*) of the trough axis, there is positive (*negative*) geostrophic vorticity advection. In the absence of other processes, PVA is associated with height falls ($\chi < 0$) while NVA is associated with height rises ($\chi > 0$). Since the geostrophic vorticity advection is precisely zero at the *axis* of the trough (since the gradient of geostrophic vorticity is zero there), there is no height tendency at that point. Thus, the geostrophic vorticity advection term can only propagate an already existing disturbance, it cannot intensify it—that is, it does not contribute to cyclogenesis.

The second term on the RHS of (3) can be rewritten as
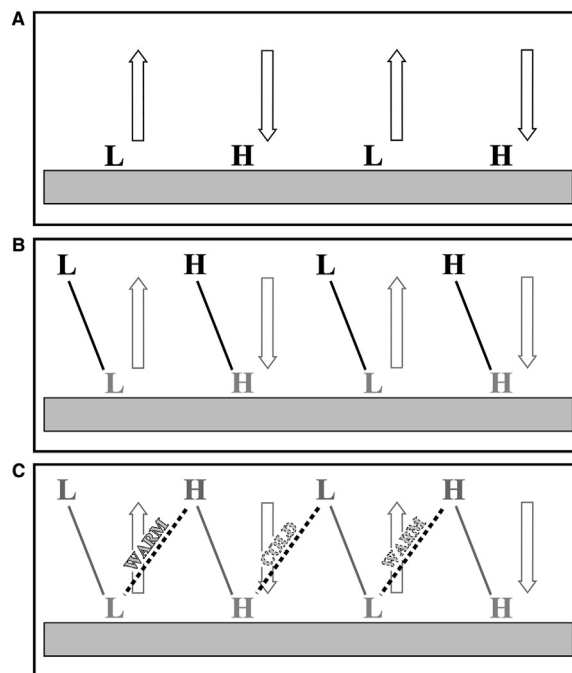
Fig. 7 Vertical structure of a developing mid-latitude cyclone, (A) Alternating sequence of surface high and low pressure systems with ascent (descent) slightly downstream from the lows (highs). (B) Upper tropospheric lows and highs are displaced to the west with height (see text for explanation). Thick solid lines represent geopotential axes connecting surface and upper tropospheric features. (C) Thick dashed lines are thermal axes which tilt slightly to the east with height (see text for explanation). Note that warm air is ascending and cold air is descending in this wave train. Adapted from Martin (2006).
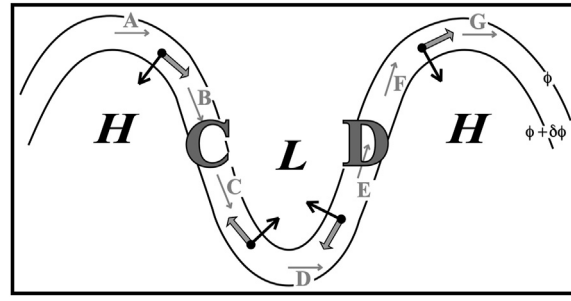
Fig. 8 Schematic upper tropospheric trough/ridge wave train in which the speed of the flow is the same everywhere. Thick black arrows represent the acceleration vectors, $\frac{d\vec{V}}{dt}$, at the indicated points determined graphically by finite differencing between adjacent wind arrows (in gray). Gray shaded arrows represent resultant ageostrophic winds, $\vec{V}_{ag}$, at the indicated points. Convergence and divergence are indicated by the "C" and "D", respectively. Adapted from Martin (2006).

$$-\frac{f_o^2}{\sigma} \frac{\partial}{\partial p}\left[-\overrightarrow{V_g} \cdot \nabla\left(-\frac{\partial\phi}{\partial p}\right)\right]. \tag{4A}$$

Since $-\frac{\partial\phi}{\partial p} = \frac{RT}{p}$ and $-\frac{\partial}{\partial p}$ represents the vertical derivative, (4A) can be expressed as

$$\frac{Rf_o^2}{p\sigma}\left[-\frac{\partial}{\partial p}\left(-\overrightarrow{V_g} \cdot \nabla\mathrm{T}\right)\right], \tag{4B}$$

the vertical derivative of geostrophic temperature advection. This term controls the *development* of disturbances from the perspective of the QG height tendency equation as geostrophic temperature advection increasing (*decreasing*) upward is associated with height falls (*rises*). In a developing extratropical cyclone it is often observed that middle tropospheric height rises (manifest as ridge building) typically occur to the east of the sea-level pressure (SLP) minimum, in the vicinity of the cyclone's warm front. From the tendency equation perspective, this is a result of the fact that warm air advection is strong in the lower troposphere and weaker in the middle and upper troposphere in that region of the storm. The result is warm air advection decreasing with height and height rises. To the west of the SLP minimum, middle tropospheric height falls occur consistent with the fact that lower tropospheric cold air advection associated with the surface cold front is stronger than the middle and upper tropospheric cold air advection in the same location. Thus, the geostrophic temperature advection increases with height there, leading to mid-tropospheric height falls. The height falls to the west of the developing SLP minimum lead to a positive, mid-tropospheric geostrophic vorticity tendency there while the height rises to the east of the SLP minimum are associated with a negative, mid-tropospheric geostrophic vorticity tendency there, as illustrated in Fig. 10. The juxtaposition of positive and negative geostrophic vorticity tendencies, in turn, promotes an decrease in vorticity along the thermal wind above the surface cyclone—a fundamental forcing for the production of synoptic-scale upward vertical motions as will be shown presently.

Beginning again with

$$\frac{\partial \zeta_g}{\partial t} = -\overrightarrow{V_g} \cdot \nabla\left(\zeta_g + f\right) + f_o\frac{\partial\omega}{\partial p}$$

$$\frac{\partial}{\partial t}\left(-\frac{\partial\phi}{\partial p}\right) = -\overrightarrow{V_g} \cdot \nabla\left(-\frac{\partial\phi}{\partial p}\right) + \sigma\omega$$
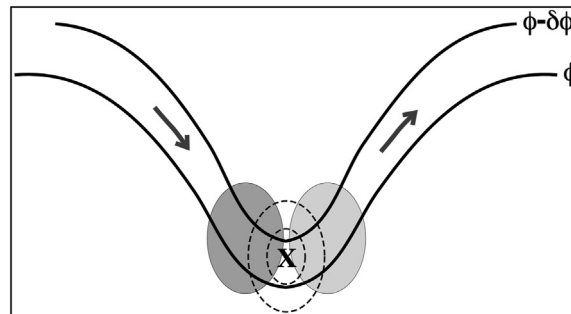
Fig. 9 Upper tropospheric trough in the Northern Hemisphere. Thick black lines are isopleths of geopotential. Gray arrows are geostrophic wind vectors and the dashed lines are contours of cyclonic vorticity with the "X" indicating the vorticity maximum. Light (dark) shading represents region of positive (negative) vorticity advection. Adapted from Martin (2006).
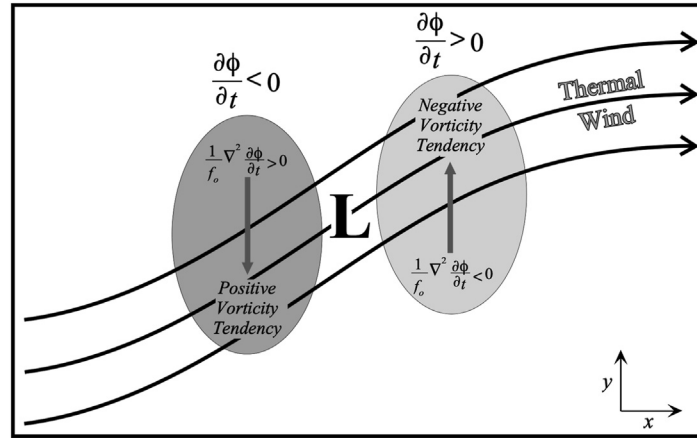
Fig. 10 The effect of horizontal temperature advection on geopotential tendency. Solid black arrows are streamlines of the lower tropospheric thermal wind. Surface low pressure center is indicated with "L" and the gray arrows represent the lower tropospheric winds associated with the storm. Light (dark) shaded region identifies an area where warm (cold) air advection decreases with height leading to height rises (falls) and a negative (positive) vorticity tendency. Adapted from Martin (2006).

but with the goal of eliminating reference to $\frac{\partial \phi}{\partial t}$, adding $f_o \frac{\partial}{\partial p}(1A)$ to $\nabla^2(2A)$ yields

$$0 = f_o \frac{\partial}{\partial p}\left[-\overrightarrow{V}_g \cdot \nabla(\zeta_g + f)\right] + f_o^2 \frac{\partial \omega^2}{\partial p^2} + \nabla^2\left[-\overrightarrow{V}_g \cdot \nabla\left(-\frac{\partial \phi}{\partial p}\right)\right] + \sigma \nabla^2 \omega \qquad (5A)$$

which can be rearranged into

$$\sigma\left(\nabla^2 + f_o^2 \frac{\partial^2}{\partial p^2}\right)\omega = f_o \frac{\partial}{\partial p}\left[\overrightarrow{V}_g \cdot \nabla(\zeta_g + f)\right] + \nabla^2\left[\overrightarrow{V}_g \cdot \nabla\left(-\frac{\partial \phi}{\partial p}\right)\right] \qquad (5B)$$

known as the *quasi-geostrophic omega equation*. Note that (5B) is a diagnostic equation for ω in terms of the instantaneous geopotential height field. Thus, it affords a reasonable estimate of ω without direct observations of the wind. An equivalent form of this expression, derived by Hoskins et al. (1978), is given by

$$\sigma\left(\nabla^2 + f_o^2 \frac{\partial^2}{\partial p^2}\right)\omega = -2\nabla \cdot \overrightarrow{Q} \qquad (6)$$

where $\overrightarrow{Q}$ is given by

$$\overrightarrow{Q} = f\gamma\left[\left(-\frac{\partial \overrightarrow{V}_g}{\partial x} \cdot \nabla\theta\right)\widehat{i}, \left(-\frac{\partial \overrightarrow{V}_g}{\partial y} \cdot \nabla\theta\right)\widehat{j}\right] \qquad (7)$$

with f as the Coriolis parameter and $\gamma = \frac{R}{fP_o}\left(\frac{p_o}{p}\right)^{c_v/c_p}$ (or $\gamma = -\frac{1}{f\theta}\frac{\partial \phi}{\partial p}$). This so-called $\overrightarrow{Q}$-vector form of the QG ω-equation affords enhanced physical interpretation compared to the traditional form of the expression.[2] A good deal of this insight arises from the fact that $\overrightarrow{Q}$ has an additional physical meaning—namely,

$$\overrightarrow{Q} = f\gamma \frac{d}{dt_g}\nabla\theta \qquad (8)$$

where $\frac{d}{dt_g}\nabla\theta$ represents the Lagrangian rate of change of the vector $\nabla\theta$ following the geostrophic flow.

This property of $\overrightarrow{Q}$ can be exploited in pursuit of insights regarding the extratropical cyclone. It is instructive to partition a given $\overrightarrow{Q}$-vector into its across- and along-isentrope components. As shown schematically in Fig. 11, the across-isentrope component, $\overrightarrow{Q}_n$, can only affect changes in the magnitude of $\nabla\theta$. Meanwhile, $\overrightarrow{Q}_s$, which is directed perpendicularly to $\nabla\theta$, can only affect changes in the direction of $\nabla\theta$. Simple vector calculus provides expressions for both $\overrightarrow{Q}_n$ and $\overrightarrow{Q}_s$ as

---

[2]A detailed conceptual/mathematical derivation of the Q-vector form of the QG ω-equation is offered in Martin (2006), p. 166−181.
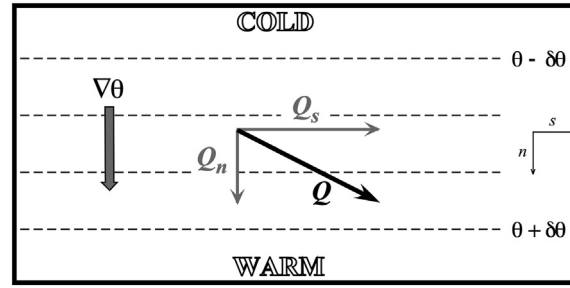
Fig. 11 Natural coordinate partition of the **Q**-vector into its along-isentrope (**Q$_s$**) and across-isentrope (**Q$_n$**) components. See text for explanation. Adapted from Martin (2006).

$$\vec{Q}_n = \left(\frac{\vec{Q}\cdot\nabla\theta}{|\nabla\theta|}\right)\left(\frac{\nabla\theta}{|\nabla\theta|}\right) \tag{9}$$

$$\vec{Q}_s = \left(\frac{\vec{Q}\cdot\left[\hat{k}\times\nabla\theta\right]}{|\nabla\theta|}\right)\left(\frac{\hat{k}\times\nabla\theta}{|\nabla\theta|}\right) \tag{10}$$

since $\left|\hat{k}\times\nabla\theta\right| = |\nabla\theta|$. Clearly, the full $\vec{Q}$-vector is given by the sum

$$\vec{Q} = \vec{Q}_n + \vec{Q}_s \tag{11}$$

and so the forcing for ω is, likewise, represented by the sum

$$-2\nabla\cdot\vec{Q} = -2\nabla\cdot\vec{Q}_n - 2\nabla\cdot\vec{Q}_s \tag{12}$$

The resulting pieces of the total ω field will appear as couplets straddling the thermal wind ($-2\nabla\cdot\vec{Q}_n$, *transverse* couplets) and along the thermal wind ($-2\nabla\cdot\vec{Q}_s$, *shearwise* couplets), respectively. Since $\vec{Q}_n$ only impacts the magnitude of $\nabla\theta$, $-2\nabla\cdot\vec{Q}_n$ forces couplets of vertical motion that are directly related to geostrophic horizontal frontogenetic processes. That means that all of the non-frontogenetically forced vertical motions in the cyclone environment arise from the $-2\nabla\cdot\vec{Q}_s$ forcing term.

Keyser et al. (1988) showed that

$$\frac{\vec{Q}\cdot\left(\hat{k}\times\nabla\theta\right)}{|\nabla\theta|} = \frac{f\gamma}{2}|\nabla\theta|\left[\zeta_g + E sin2\beta\right] \tag{13}$$

Where ζ_g is the geostrophic vorticity, E is the total geostrophic deformation and β is the angle between the isentropes and the local axis of dilatation of the deformation field. Given these relationships,

$$-2\nabla\cdot\vec{Q}_s = -2f\gamma\nabla\cdot\left[\left(\frac{\vec{Q}\cdot\left(\hat{k}\times\nabla\theta\right)}{|\nabla\theta|}\right)\left[\frac{\hat{k}\times\nabla\theta}{|\nabla\theta|}\right]\right] \tag{14A}$$

$$= f\gamma\nabla\cdot\left[|\nabla\theta|(\zeta_g + Esin2\beta)\left[\frac{\hat{k}\times\nabla\theta}{|\nabla\theta|}\right]\right] \tag{14B}$$

$$= -f\gamma\left[\hat{k}\times\nabla\theta\right]\nabla\cdot\left(\zeta_g + Esin2\beta\right) \tag{14C}$$

and since,

$$\gamma\left[\hat{k}\times\nabla\theta\right] = -\gamma\frac{\partial\theta}{\partial y}\hat{i} + \gamma\frac{\partial\theta}{\partial x}\hat{j} = -\frac{\partial u_g}{\partial p}\hat{i} - \frac{\partial v_g}{\partial p}\hat{j} \tag{15}$$

Then

$$-2\nabla\cdot\vec{Q}_s = -f\vec{V}_T\cdot\nabla\zeta_g - f\vec{V}_T\cdot\nabla(Esin2\beta) \tag{16}$$

The first term on the RHS of (16) represents the thermal wind advection of geostrophic vorticity, recognized as the predominant forcing for synoptic-scale vertical motions as far back as the pioneering work on development by Sutcliffe (1947), later reiterated by Trenberth (1978).

Armed with both the QG height tendency and omega equations, the physical sequence of events that characterize the adjustment of the mass and temperature fields to a canonical cyclogenesis event can be considered. Nearly all cyclogenesis events proceed from a precursor upper level disturbance in the flow. This disturbance often manifests itself as a relative vorticity maxima as illustrated in **Fig. 12**A. Given the influence of vorticity advection in the tendency equation, the disturbance will propagate in the direction of the flow. The zonal thermal wind depicted in **Fig. 12**A implies a positive (*negative*) vorticity advection by the thermal wind downstream (*upstream*) of the disturbance. From the QG omega equation, this circumstance is associated with upward (*downward*) vertical motion downstream (*upstream*) of the trough axis as shown in **Fig. 12**B. An alternative way to view this forcing for vertical motion is through the partitioned $\vec{Q}$-vector perspective. Since $-f\vec{V}_T \cdot \nabla\zeta_g$ can be written as $-f\nabla \cdot (\vec{V}_T\zeta_g)$ (because $\nabla \cdot \vec{V}_T = 0$), this forcing can be expressed in terms of the divergence of a vector field oriented parallel to the thickness isopleths as shown. Consequently, the initial vertical motion couplet portrayed in **Fig. 12**B is a *shearwise* couplet. Shearwise vertical motions, by virtue of their relation to the $\vec{Q}_s$ component of the $\vec{Q}$-vector, are associated with rotation of the $\nabla\theta$ vector. Thus, the schematic distribution of $\vec{Q}_s$ shown in **Fig. 12**B will also deform the thermal field, producing a thermal ridge downstream of the upper-level trough axis (in the vicinity of the developing surface low pressure center) and a thermal trough upstream as shown in **Fig. 12**C. Under the influence of the cyclonic circulation associated with the developing lower tropospheric disturbance, low-level warm air advection will occur downstream of the upper-level trough axis and low-level cold air advection just upstream of it. As illustrated in **Fig. 10**, the tendency equation suggests that such a circumstance will serve to raise the geopotential heights in the middle troposphere to the east of the surface low and lower the heights to its west. The resulting increased gradient of vorticity along the thermal wind leads to greater PVA by the thermal wind and attendant upward vertical motions which further intensify the surface cyclone downstream of the upper feature. In this way, the asymmetric temperature field associated with a developing mid-latitude cyclone makes a significant contribution to the dynamics of cyclogenesis. The rotation of $\nabla\theta$ afforded by the shearwise vertical motions eventually orients the baroclinicity into a configuration in which the deformation fields characteristic of the cyclogenesis itself begin to locally increase $|\nabla\theta|$. Thus, the cold and warm frontal zones begin to develop along with their frontogenetically-induced *transverse* circulations which tend to be linear and oriented along the warm and cold fronts. The combination of the shearwise and transverse couplets of vertical motion thus produced underlies the comma-shaped cloud distribution that characterizes the mid-latitude cyclone.
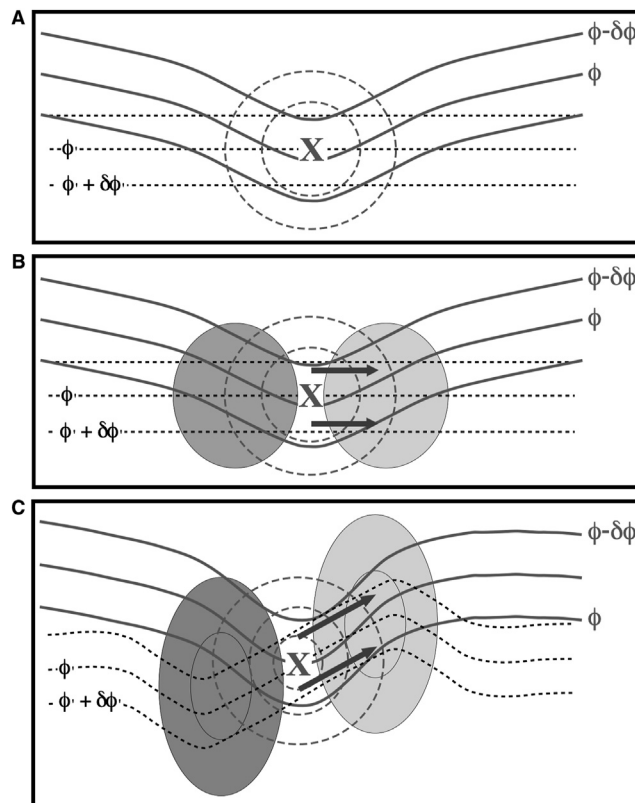
Fig. 12   Initial thermal and mass field adjustments to cyclogenesis. (A) Upper tropospheric vorticity maxima in a zonal thermal wind. Gray solid lines are 500 hPa geopotential heights, dashed gray lines are 500 hPa geostrophic absolute vorticity, and the black dashed lines are 1000−500 hPa thickness isopleths. "X" marks the location of the maximum absolute vorticity. (B) As for Fig. 12a with the gray arrows representing the $\boldsymbol{Q_{TR}}$ vectors. Light (dark) shaded area is a region of upward (downward) vertical motion and upper tropospheric divergence (convergence). (C) As for **Fig. 12**B but for a subsequent time in the cyclone's development. Note the development of the thermal ridge downstream of the upper trough axis and the thermal trough upstream of it. Larger $\boldsymbol{Q_{TR}}$ vectors and greater vertical motions are the result of intensification of the 500 hPa trough/ridge couplet. Adapted from Martin (2006).
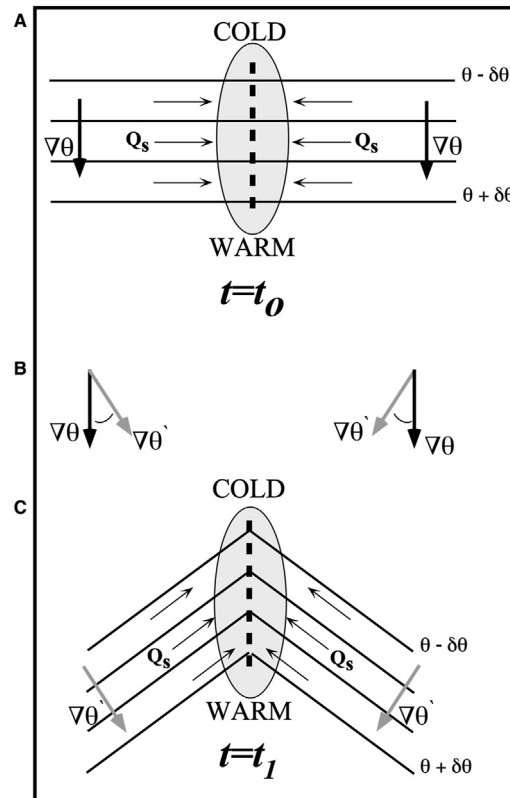
Fig. 13 The effect of $\mathbf{Q_s}$ convergence on horizontal thermal structure. (A) Straight line isentropes (solid lines) in a field of $\mathbf{Q_s}$ convergence (shading). Thick dashed line indicates axis of maximum $\mathbf{Q_s}$ convergence. Direction of $\nabla\theta$ vector on either side of the $\mathbf{Q_s}$ convergence maximum is indicated. (B) Rotation of $\nabla\theta$ vector implied by $\mathbf{Q_s}$ vectors on either side of the $\mathbf{Q_s}$ convergence maximum in **Fig. 13**A. Thick black arrow denoted as $\nabla\theta$ represents the original direction of the $\nabla\theta$ vector. Thick gray arrow denoted as $\nabla\theta'$ represents direction of $\nabla\theta$ vector after rotation implied by $\mathbf{Q_s}$ vectors. (C) Orientation of the baroclinic zone depicted in **Fig. 13**A after differential rotation of $\nabla\theta$ on either side of the $\mathbf{Q_s}$ convergence maximum. Adapted from Martin (2006).

Finally, it should be noted that the along-isentrope component of $\overrightarrow{Q}$ offers insight into the process of occlusion. **Fig. 13**A illustrates a straight baroclinic zone along which there is a region of convergence of $\overrightarrow{Q}_s$. This convergence will not only be associated with upward vertical motion, a consequence of the quasi-geostrophic omega equation, but will also differentially rotate $\nabla\theta$ on either side of the convergence axis, as illustrated in **Fig. 13**B. Since $\overrightarrow{Q}_s$ cannot change the magnitude of $\nabla\theta$, the result is displayed in **Fig. 13**C—the production of a thermal ridge characterized by upward vertical motion. **Fig. 14** shows the partition of the total 500:900 hPa column averaged $\overrightarrow{Q}$-vector forcing (**Fig. 14**A) in the occluded sector of a post-mature extratropical cyclone. It is clear that the $\overrightarrow{Q}_s$ component (**Fig. 14**B) far exceeds the $\overrightarrow{Q}_n$ component (**Fig. 14**C) in that region. This turns out to be characteristic of occluded extratropical cyclones. Thus, rotation of $\nabla\theta$ by the geostrophic flow (described by $\overrightarrow{Q}_s$) is the underlying dynamical mechanism responsible for creating the occluded thermal structure and for forcing the quasi-geostrophic ascent associated with that process in the occluded sector of cyclones.[3]

As the upper disturbance continues to develop and progress eastward, it begins to outrun its surface reflection. As a result, the convergence at the surface (maximized at the location of the sea-level pressure minimum as a result of boundary layer friction) gradually becomes disconnected from its divergence valve aloft and the surface cyclone can no longer intensify. Thus, the phasing of the upper and lower disturbances is crucial to development.

The Influence of Diabatic Effects

The foregoing description of cyclogenesis makes no mention of the fact that clouds and precipitation (and therefore latent heat release) are involved in this process. Naturally, the interaction between the dynamic and diabatic processes is an important aspect

---

[3]Further analysis of the $\overrightarrow{Q}_s$ component of this forcing by Martin (1999) extends the physical insight regarding the process of occlusion in extratropical cyclones.
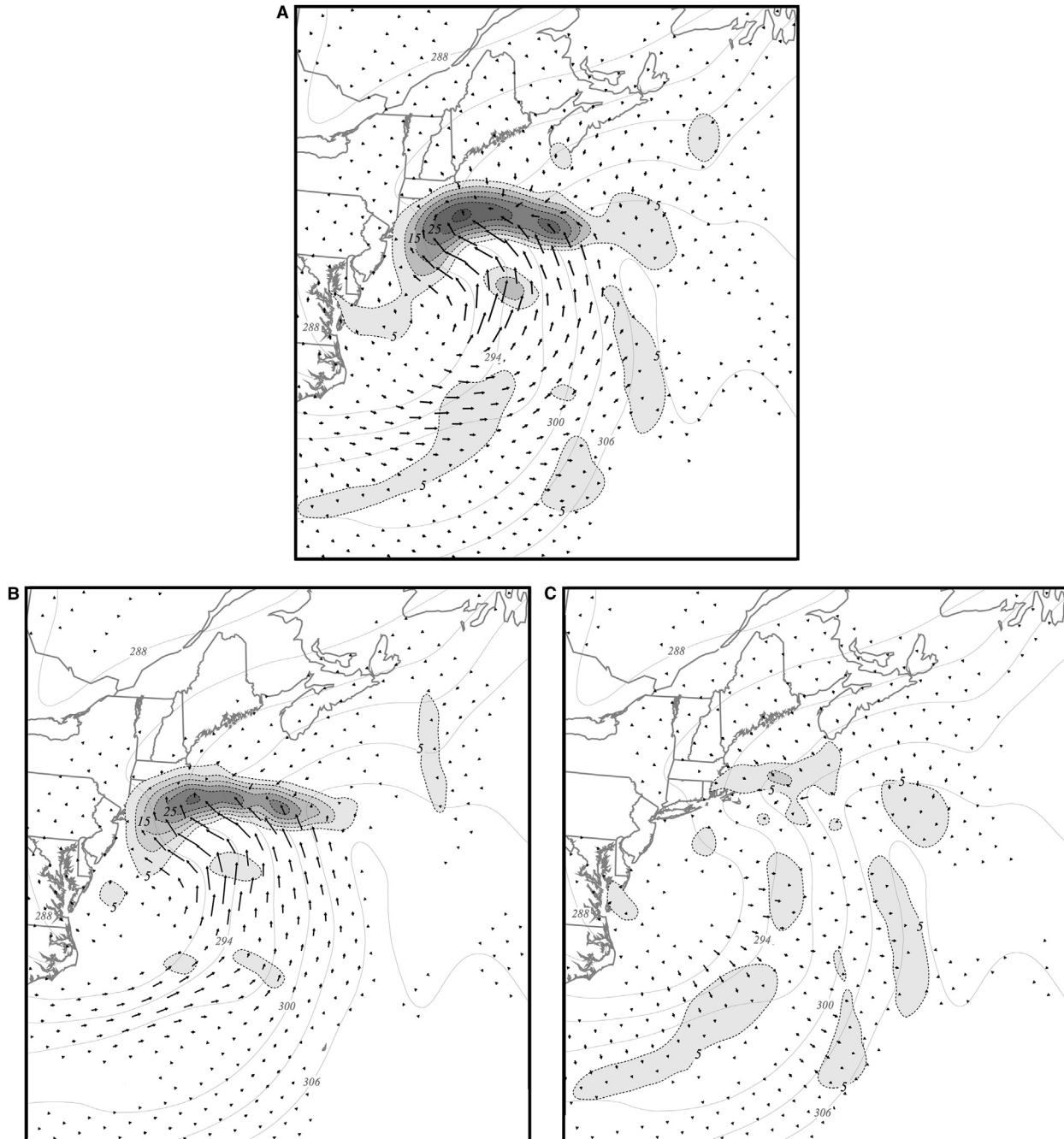
Fig. 14   (A) 500:900 hPa column averaged **Q**-vectors and **Q**-vector convergence from an 18 h forecast of the NCEP Eta model valid at 0600 UTC April 1, 1997. Q convergence is contoured and shaded in units of m kg^{-1} s^{-1} every 5×10^{-16} m kg^{-1} s^{-1} beginning at 5×10^{-16} m kg^{-1} s^{-1}. Thin gray lines are 500:900 hPa column averaged isentropes labeled in K and contoured every 3 (K) (B) As in (A) except for **Q$_s$**. (C) As in (A) except for **Q$_n$**. Adapted from Martin (2006).

of the overall process of cyclogenesis. Though such interaction characterizes every cyclogenesis event to some degree, these interactions are most vividly illustrated by considering cases of dramatic surface development, known as explosive cyclogenesis.

Explosive cyclogenesis is the term of art that describes the rapid development of a sea-level pressure minimum. Pioneering work on this subject by Sanders and Gyakum (1980) has suggested a threshold of 24 hPa of deepening in 24 hours[4] as a reasonable distinguishing characteristic of an explosive deepener. The deepening rates for all Northern Hemisphere cyclones in a single year is shown in Fig. 15. The rapid deepeners appear to account for a muted second peak in the overall distribution suggesting that

---

[4]This value was suggested by Sanders and Gyakum (1980) and is normalized for latitude according to the following formula; *Deepening Rate* $= \Delta p \left(\frac{\sin \phi}{\sin 60^\circ} \right)$.
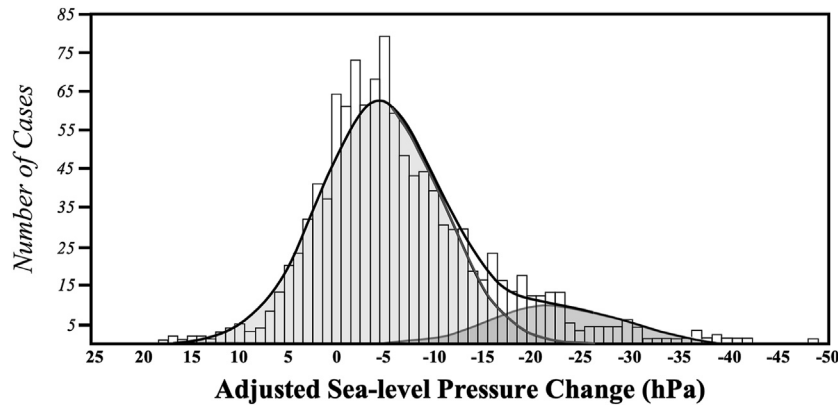
Fig. 15 Distribution of 24 h deepening rates for all Northern Hemisphere surface cyclones in one year. The dark solid line indicates the sum of two normal curves while the gray lines and shadings represent the separate distributions (light shading for the "ordinary" and darker for "explosive" cyclones). Adapted from Roebber (1984).

something may be different about these storms. In fact, there are some notable differences between the "ordinary" cyclones that constitute the majority of all cyclones and these less common events. One such difference is that the explosive deepeners not only deepen more rapidly but also for a longer time than the "ordinary" cyclones. What does this mean about the contrast in physical processes that operate in these two populations? The hemispheric distribution of these explosive deepeners provides a first order clue as to the circumstances that conspire to produce them. As illustrated in Fig. 16, Northern Hemisphere explosive cyclogenesis events tend to occur along the warm western boundary ocean currents such as the Kurishio and Gulfstream. The prevailing view is that these developments are forced by the same physical and dynamical processes that occur to some degree in all cyclones but act with particular vigor in explosive deepeners. It is reasonable to wonder what makes ordinary processes so potent in these storms. The fact that surface development is strongly tied to upward vertical motion (via the column stretching described in the vorticity equation) compels another look at the QG omega equation.

$$\sigma\left(\nabla^2 + f_o^2 \frac{\partial^2}{\partial p^2}\right)\omega = -2\nabla \cdot \overrightarrow{Q}$$

Consider, hypothetically, two days on which the RHS forcing $(-2\nabla \cdot \overrightarrow{Q})$ in a given domain is exactly the same. Given this circumstance, only the static stability (σ) could possibly influence the production of stronger vertical motions on one day versus the other. In fact, σ acts as the amplitude modulator of the omega equation; lower (*higher*) σ is associated with a greater (*lesser*) response to a given forcing.

Thus, to first order, the prevalence of explosively deepening cyclones over warm ocean currents is a result of the fact that these locations are characterized by consistently lower static stability and, consequently, a consistently more vigorous response to forcing
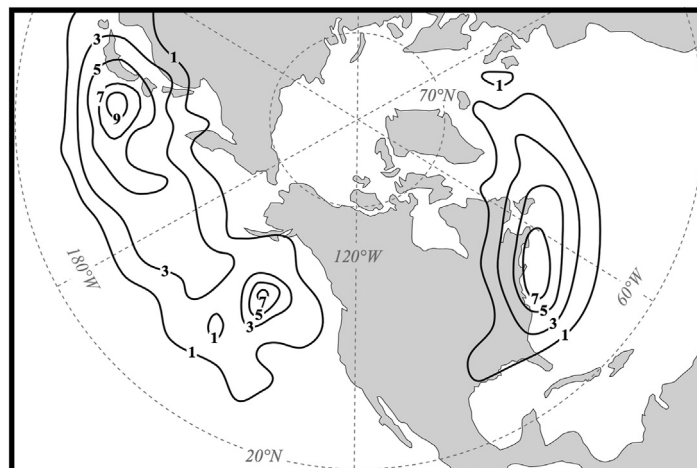
Fig. 16 Geographical distribution of positions of maximum deepening for all Northern Hemisphere cyclones from 1976—1982 that intensified at a rate greater than 24 hPa (24 h)$^{-1}$. Numbers indicated the annual frequency of such developments at at the indicated locations. Adapted from Roebber (1984).
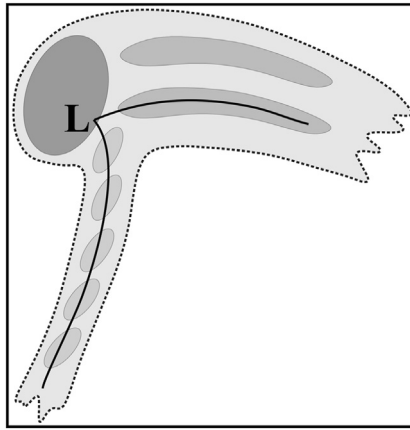
Fig. 17 Schematic depicting the asymmetric cloud and precipitation distribution in a typical mid-latitude cyclone. The lightly shaded area enclosed by the dashed line is the cloud pattern. The solid lines within that region are the surface cold and warm fronts. The shaded subregions within the cloud mass are the precipitation elements associated with the cold front (lightest shading), warm front (darker shading), and the area to the north and northwest of the surface cyclone center (darkest shading). Adapted from Martin (2006).

for upward vertical motion. These more intense vertical motions then lead to more intense cyclogenesis. But even this physical linkage does not yet reference the effect of the characteristic cloud and precipitation distribution of cyclones.

The characteristic asymmetric precipitation distribution associated with extratropical cyclones is illustrated schematically in Fig. 17. The period of most rapid development often occurs when heavy precipitation develops poleward and westward of the cyclone center. The attendant latent heat release (LHR) (1) adds energy to the system, (2) focuses and intensifies the vertical motion pattern through a local reduction of the static stability in saturated updrafts, and, perhaps most interestingly, (3) affects the structure and dynamics of the larger-than-cyclone scale so as to intensify the cyclogenetic effect of ordinary dynamical processes. This last point lies at the heart of a conceptual/dynamical model of cyclogenesis known as the "self development" paradigm. Consider, as a first example, the cyclogenetic feedback from sensible and latent heat fluxes in the lower troposphere. As shown schematically in Fig. 18, poleward directed boundary layer winds coupled with ascent on the eastern side of the cyclone warm the lower troposphere on the equatorward side of the developing warm front through both sensible heating associated with the warm air advection and diabatic heating resulting from latent heat release in the moist, ascending air. This warming leads to an increase in the magnitude of the low-level temperature gradient and a consequent increase in the magnitude of the warm advection there. Stronger warm advection is often associated with intensified ascent in that location. Greater ascent leads to more intense baroclinic energy conversion and often to a stronger cyclone whose intensified circulation contributes to a positive feedback loop.

On larger scales, the LHR associated with cloud and precipitation production produces a positive thickness anomaly just east of the upper-level shortwave trough axis (Fig. 19). Consequently, the geopotential heights in the middle and upper troposphere increase there and a small-scale ridge is built up above the latent heating maxima. Positive vorticity advection to the east of the upper-level shortwave compels that feature to move eastward. In the face of the diabatic ridge building that occurs in association with the LHR in the cloud shield to the east, the wavelength between the upstream trough and downstream ridge axes shrinks. As a result of this wavelength shortening, and the associated increase in the upper-tropospheric vorticity gradient, the magnitude of the cyclonic vorticity advection by the thermal wind downstream of the trough axis greatly intensifies leading to more intense upward vertical motions. The stronger vertical motions intensify the cyclogenesis and produce more LHR just downstream of the upper-level shortwave which tends to further shorten the wavelength of the upper-disturbance. In this way, an additional positive feedback loop is established.
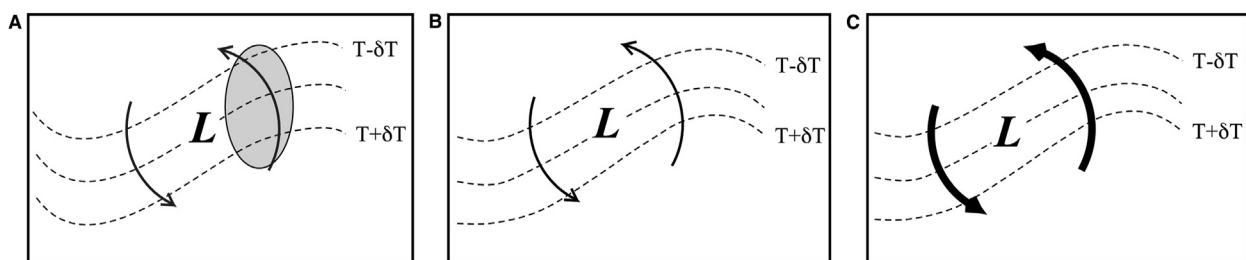
Fig. 18 Schematic illustration of the influence sensible and latent heat fluxes in the planetary boundary layer can have on the magnitude of the lower tropospheric temperature advection east of the surface cyclone center. (A) Prior to the influence of the heat fluxes a uniform temperature gradient exists. Dashed lines are isotherms, "L" is the location of the sea-level pressure minimum, arrows represent the flow around the cyclone and the gray shaded area is the location where heat fluxes will warm the boundary layer. (B) Increased temperature gradient results from the heating in the boundary layer. Intensified lower tropospheric wann air advection intensifies the cyclone. (C) More intense cyclone leads to more intense lower tropospheric winds (bolder arrows) and increased warm air advection. Adapted from Martin (2006).
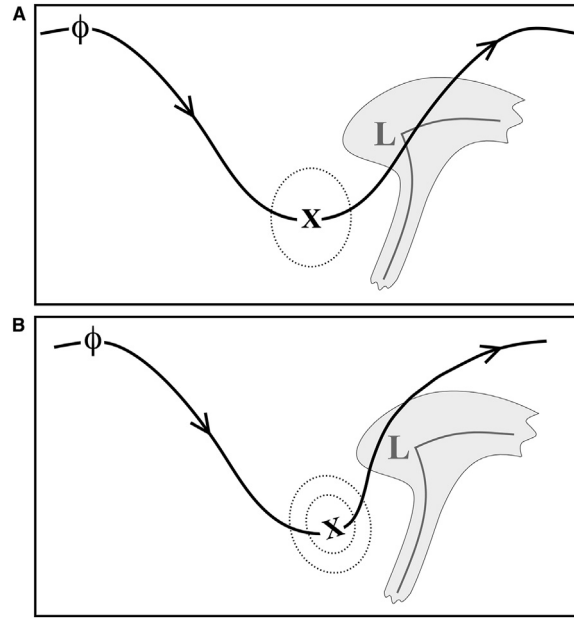
Fig. 19 Schematic illustrating how latent heat release associated with the developing cloud and precipitation shield of a midlatitude cyclone feeds back on the development. (A) Initial upper tropospheric wave in a geopotential height contour with the upper tropospheric vorticity maxima indicated by the "X." Surface low, and associated cloud and precipitation, develops downstream of "X." (B) Latent heat release associated with the cloud and precipitation shield increases column thicknesses downstream of the upper vorticity maxima deforming the upper tropospheric geopotential as indicated. The result is a more significant ridge downstream of the upper trough and greater curvature vorticity in the vicinity of the upper trough axis as indicated. Adapted from Martin (2006).

A large number of numerical modeling studies investigating the influence of LHR on cyclogenesis have been undertaken in the past 50 years. The consensus conclusion drawn from these studies is that since water vapor is not a passive scalar, its phase change tends to concentrate normal baroclinic processes onto smaller scales which leads to feedbacks that further the scale contraction and intensification of these explosively deepening storms. From that perspective, it becomes clear that these storms do not arise as a consequence of "special" dynamical processes but rather as a result of uncommonly intense interactions among the "ordinary" suite of physical and dynamical processes that operate, to some degree, in all mid-latitude cyclones.

Cyclogenesis from the Potential Vorticity (PV) Perspective

The foregoing discussion of cyclogenesis has been conducted from what might be called the "basic state variables" perspective in which a number of separate variables are considered simultaneously in the context of the physical relationships and mathematical expressions relating them. A different, but complimentary, discussion of the process of cyclogenesis can also be had from the perspective of tracing a single variable, the potential vorticity (PV). Interest in PV proceeds from the curious relationship between vorticity and static stability in isentropic (θ) coordinates. By virtue of their invariance, the physical connection between vorticity and divergence is, as in all other coordinate systems, manifest in the isentropic coordinate vorticity equation,

$$\frac{d(\zeta_\theta + f)}{dt} = -(\zeta_\theta + f)\left(\nabla \cdot \overrightarrow{V}_\theta\right) \tag{17}$$

So long as the flow is adiabatic parcels cannot pass through isentropes. In such a flow, horizontal convergence in an isentropic layer of depth $\delta\theta$ leads to an increase in mass ($-\frac{1}{g}\frac{\delta p}{\delta\theta}$) in that layer. This relationship is formalized in the continuity equation in θ-coordinates,

$$\frac{d}{dt}\left(-\frac{1}{g}\frac{\partial p}{\partial\theta}\right) = -\left(-\frac{1}{g}\frac{\partial p}{\partial\theta}\right)\left(\nabla \cdot \overrightarrow{V}_\theta\right) \tag{18}$$

Equating the expressions for $(\nabla \cdot \overrightarrow{V}_\theta)$ in (17) and (18), and integrating from an initial time to a later time[5] leads to the conclusion that the quantity

---

[5]Details of this derivation can be found in Martin (2006), p. 276–277.
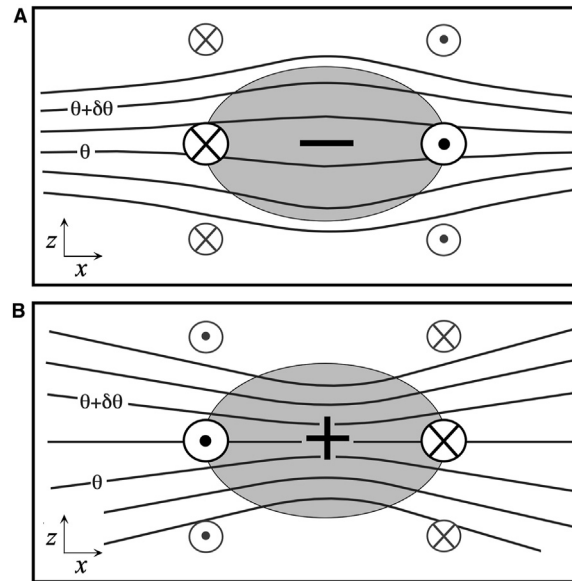
Fig. 20 (A) Characteristic structure of a negative PV anomaly. Gray shaded area delineates the negative anomaly and thin solid lines are isentropes. Wind into the page is indicated by an "X" while wind out of the page is signified by the dot. (B) Characteristic structure of a positive PV anomaly. Adapted from Martin (2006).

$$-g(\zeta_\theta + f)\left(\frac{\partial \theta}{\partial p}\right) \tag{19}$$

known as the isentropic potential vorticity (IPV), is constant in adiabatic flow.

    This important variable is called *potential vorticity* because there is a *potential* for creating relative vorticity by changing latitude (through manipulation of f) and/or by adiabatically changing the separation between isentropic levels (through manipulation of $-\frac{\partial \theta}{\partial p}$). If the flow is *not* adiabatic, as is the case in the real atmosphere, some portion of the change in a PV distribution observed over a given domain must have resulted from friction or diabatic heating—a fact that can be exploited for insight.

    Local anomalies in the PV distribution (e.g. departures from temporal or spatial averages in a given domain) are of great interest since such anomalies have identifiable and discrete circulations associated with them. In an atmosphere in thermal wind balance, a tropopause-level *negative* PV anomaly (Fig. 20A) is characterized by *negative anomalies* in both vorticity and static stability while a *positive* PV anomaly, as shown in Fig. 20B, is associated with *positive anomalies* in both the vorticity and static stability.[6] Such a feature is characterized by cyclonic flow, whose magnitude is maximized at the level of the anomaly but which extends throughout some depth above and below the anomaly according to what is known as the *penetration depth* of the anomaly, given by

$$H = \frac{fL}{N}$$

where f is the Coriolis parameter, L is the characteristic length scale of the anomaly and N is the Brunt-Vaisala frequency (a measure of static stability).

    A schematic plan-view of an upper-level PV anomaly is illustrated at two different times in Fig. 21. At the initial time (T = 0), the anomaly is represented by an equatorward protuberance of high PV air indicated by the "+" sign. Such a positive PV anomaly is associated with the cyclonic circulation indicated by the heavy arrows straddling the anomaly. The circulation will have the effect of advecting high PV southward to the west of the anomaly and low PV air northward to its east. This advection has two obvious effects; (1) to propagate the initial anomaly *upstream* (i.e. to the west), and (2) to produce a negative PV anomaly to the east of the original feature, as indicated. Notice that the phase lines of the upper-level positive PV anomaly suggests that it will propagate upstream if left to its own device. The same is true of large-scale waves (i.e. Rossby waves) which propagate westward by virtue of the fact that the meridional gradient of the Coriolis force compels positive (*negative*) planetary vorticity advection to the west (*east*) of cyclonic disturbance in the westerlies.

    In order to develop a reasonable description of cyclogenesis from the PV perspective it is also necessary to consider the structure of PV anomalies at/near the surface of the Earth. Fig. 22A shows a positive θ anomaly at the surface as might be observed ahead of a surface cold front. At the top of the atmosphere there is no vorticity since there is no wind. However, the contribution to the horizontal shear made by the warm core above the surface warm anomaly is clearly anticyclonic. Given the absence of vorticity at the top of the atmosphere and the anticyclonic *thermal* vorticity, the surface warm anomaly *has to be* a positive vorticity anomaly as well.

---

[6]This subtle but important point is proven rigorously in Martin (2006), pp. 280–282.
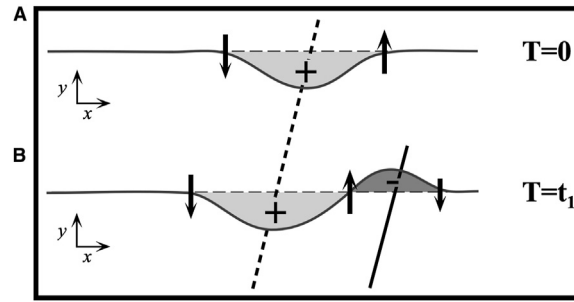
Fig. 21   (A) Positive upper tropospheric PV anomaly in the Northern Hemisphere indicated by the "+" sign and gray shading. Solid gray line is a single PV contour and the arrows indicate the cyclonic circulation associated with the PV anomaly. (B) The same PV contour at some later time. Darker shaded area with a sign indicates a negative "−" upper tropospheric PV anomaly forced by northward advection of low PV to the east of the original positive anomaly. The long dashed (solid) line is the phase line of the original positive (newly formed negative) PV anomaly. Adapted from Martin (2006).

Artificially connecting, underground, the isentropes that straddle the low-level warm anomaly, as in **Fig. 22**B, exposes it as a region of coincident positive vorticity and static stability anomalies. In other words, a low-level warm anomaly is a surrogate positive PV anomaly and can be ascribed the same characteristics as a tropopause-level positive PV anomaly. Thus, a low-level warm anomaly has a cyclonic circulation associated with it indicated by the solid arrows straddling the "+" sign in **Fig. 23**A. The southerly (*northerly*) winds downstream (*upstream*) of the anomaly center are associated with horizontal warm (*cold*) air advection. The net effect of warm advection downstream and cold advection upstream of a warm anomaly is to propagate the warm anomaly downstream, toward the warm advection and away from the cold advection (**Fig. 23**B). Only the original anomaly persists through time as there is very little upstream development in the behavior of the low-level warm anomaly.

Since the circulation associated with any PV anomaly extends through a certain depth of the atmosphere, the possibility exists that the lower tropospheric portion of the circulation associated with an upper-level PV anomaly may be able to penetrate far enough downward to influence the development of a low-level warm anomaly through horizontal advection. Likewise, the
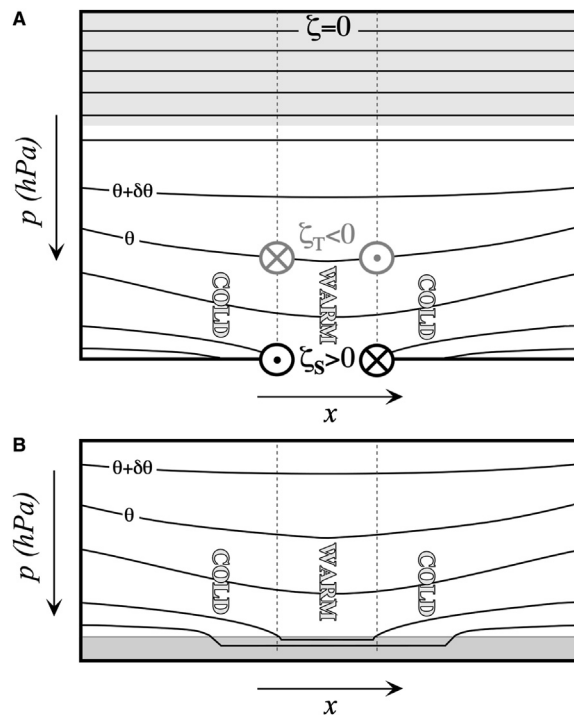
Fig. 22   Illustration of the equivalence of a surface warm anomaly to a positive PV anomaly. (A) Surface warm anomaly produces a lower tropospheric warm column within which there is anticyclonic thermal vorticity (ζ_T, indicated by light gray circles). Since there is no vorticity at the top of the atmosphere, there must be positive vorticity at the surface (ζ_S, indicated by black circles). Stratosphere is shaded gray. (B) Positive static stability anomaly is created by connecting (underground) the isentropes that straddle the warm anomaly. Surface is shaded gray. Adapted from Martin (2006).
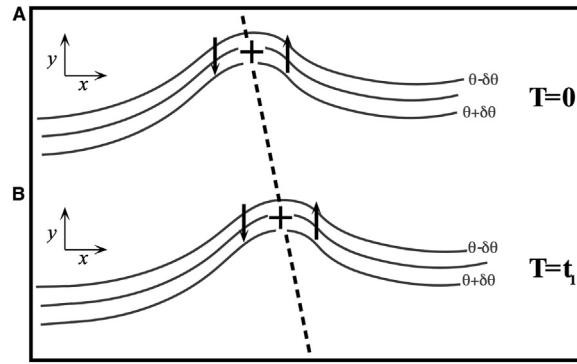
Fig. 23 (A) Schematic of a surface warm anomaly in the Northern Hemisphere. Solid gray lines are surface isentropes, "+" sign indicates the surrogate positive PV anomaly center associated with the warm anomaly, and the arrows represent the cyclonic circulation associated with the feature. (B) The same warm anomaly at some later time. The thick dashed line indicates the phase line of the warm anomaly through time. Adapted from Martin (2006).
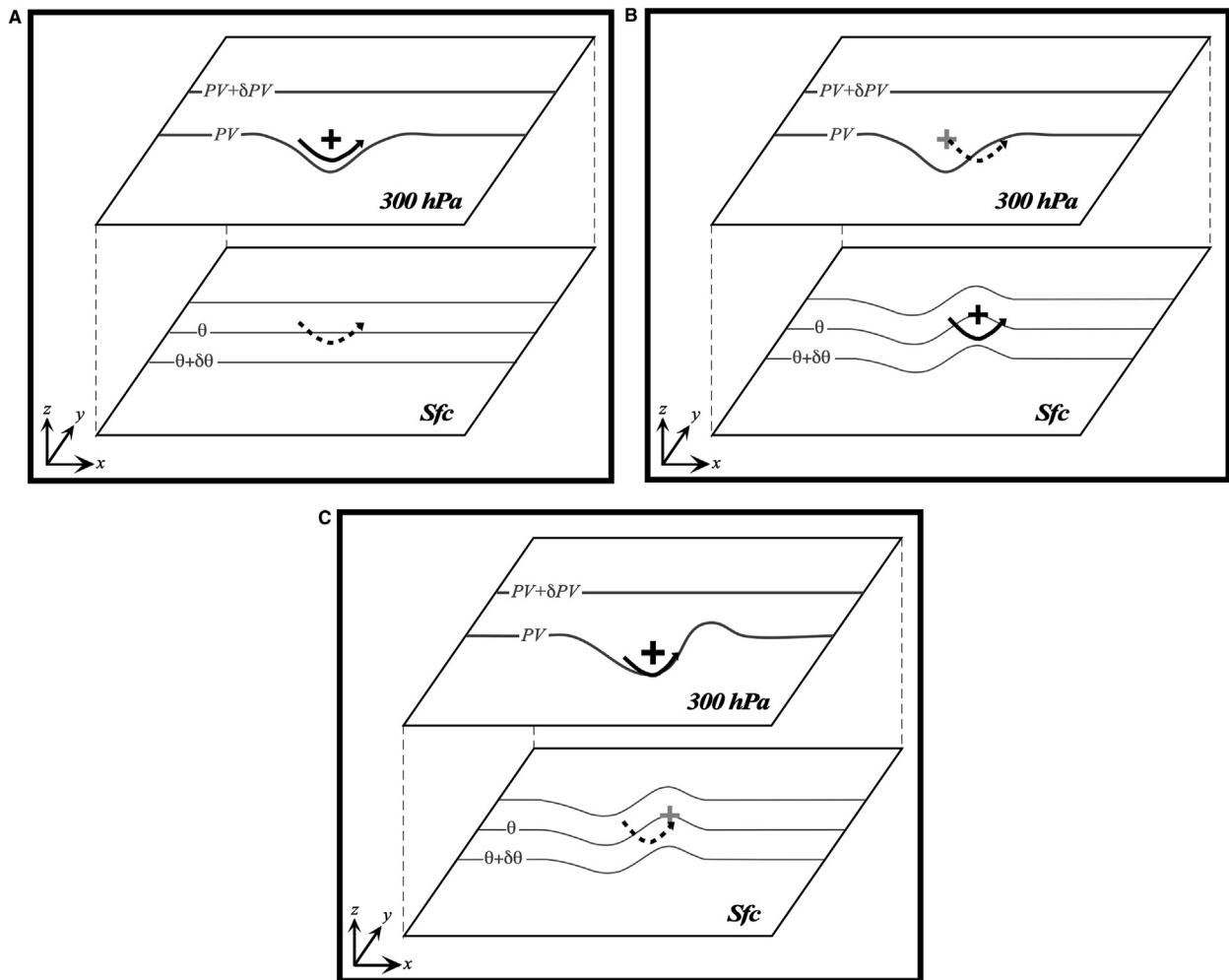
Fig. 24 Upper tropospheric positive PV anomaly moving over a low-level baroclinic zone. (A) Circulation associated with the upper PV anomaly ("+" sign) is indicated by the bold arrow. The surface reflection of that circulation is given by the dashed arrow at the surface. (B) Low-level thermal advections produce a surface warm anomaly (dark "+" sign) whose circulation, indicated by the bold arrow, has an upper tropospheric reflection (indicated by the dashed arrow). (C) Upper tropospheric PV advections intensify the upper PV anomaly (dark "+" sign) and its circulation, indicated by the bold arrow, intensifies. The surface reflection of that circulation (dashed arrow) results in thermal advections that serve to intensify the surface warm anomaly. Adapted from Martin (2006).

upper-level portion of the circulation associated with a low-level warm anomaly may penetrate far enough upward to affect the amplitude of an upper-level positive PV anomaly through horizontal PV advection at upper-levels. In short, the upper- and lower-level PV anomalies might be able to amplify one another if they are properly phased in space and situated in a not-too-strongly stratified environment. However, given the fact that the upper- and lower-level PV anomalies head in opposite directions when left to their own devices, the likelihood that prolonged mutual amplification of the separate anomalies will occur depends upon the upper- and lower-level anomalies being in sufficiently close proximity to one another for an extended period of time. Given the different propagation tendencies of the two anomalies, this would seem a difficult proposition though the difficulty is lessened by the fact that the westerly vertical shear characteristic of the mid-latitudes imposes a compensating west-to-east propagation on upper-level, synoptic-scale PV anomalies.

Fig. 24A shows an upper-level PV anomaly migrating over a lower tropospheric baroclinic zone. The upper anomaly has a cyclonic circulation associated with it that, while maximized at the level of the anomaly, extends with some vigor throughout the depth of the troposphere. The influence of the upper PV anomaly is felt at sea-level, to a degree determined by the penetration depth, in the form of a weak cyclonic circulation that acts to deform the sea-level isotherms through horizontal temperature advection (Fig. 24A). The warm air advection portion of that sea-level circulation produces a low-level warm anomaly (signified by the "+" sign in Fig. 24B) that acts as a positive PV anomaly near sea-level. This anomaly has its own circulation that, though strongest at the surface, penetrates upward through the troposphere to a degree determined by the penetration depth. Accordingly, the influence of the low-level PV anomaly is felt near the tropopause in the form of a weak cyclonic circulation that acts to intensify the upper-level PV anomaly by inducing positive PV advection into the eastern half of the anomaly. Coupled with a concurrent negative PV advection to the east of the original upper-level anomaly, this produces a tendency for the upper PV anomaly to propagate downstream, quite the opposite of its natural tendency to propagate westward. The invigorated upper-level PV anomaly then exerts an invigorated cyclonic influence on the low-level thermal field as shown in Fig. 24C. Since the upper-level PV anomaly lies upstream of the surface warm anomaly, this influence produces maximum warm air advection into the center of the warm anomaly and maximum cold air advection to its west. This distribution of surface warm and cold air advection (induced by the circulation associated with the upper-level PV anomaly) not only acts to intensify the low-level warm anomaly but also tends to promote a westward propagation of that feature, quite the opposite of its natural tendency to propagate eastward. Thus, when upper- and lower-level PV anomalies come into sufficiently close proximity, their influences on one another promote not only mutual amplification but also a beneficial "phase-locking" whereby the natural tendency for each anomaly to run away from the other is countermanded through the interaction of their respective circulations and prolonged interaction is facilitated.

Investigation of the impact of diabatic heating on cyclogenesis from the PV perspective proceeds from examination of the Lagrangian derivative of PV in isobaric coordinates, given by

$$\frac{d(PV)}{dt} = -g\left(\overrightarrow{\eta}_a \cdot \nabla \dot{\theta}\right) \tag{20}$$

where $\overrightarrow{\eta}_a$ is the three dimensional vorticity vector and $\dot{\theta}$ is the diabatic heating rate ($\frac{d\theta}{dt}$). Keeping only the vertical component,

$$\frac{d(PV)}{dt} \approx -g(\zeta+f)\frac{\partial \dot{\theta}}{\partial p} \tag{21}$$

reveals that PV is increased (*decreased*) where the vertical gradient of diabatic heating is positive (*negative*). This result is illustrated schematically in Fig. 25 in which the reasonable assumption is made that the diabatic heating maximum in a typical extratropical cyclone is located in the middle troposphere (between 400 and 600 hPa). In such a case, it is clear that PV "production" occurs in the lower troposphere while PV "destruction" occurs near the tropopause. The low-level, positive PV anomaly thus created has an
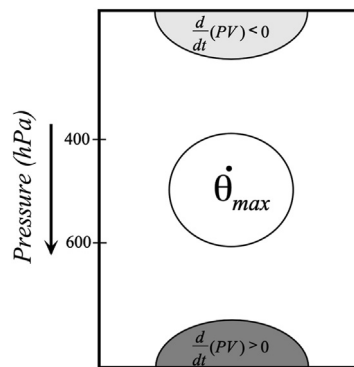
Fig. 25 Lagrangian PV tendencies associated with diabatic heating. The circle labeled $\dot{\theta}_{max}$ is the diabatic heating maximum. The light (dark) shading above (below) it indicates the region of PV destruction (production). Adapted from Martin (2006).
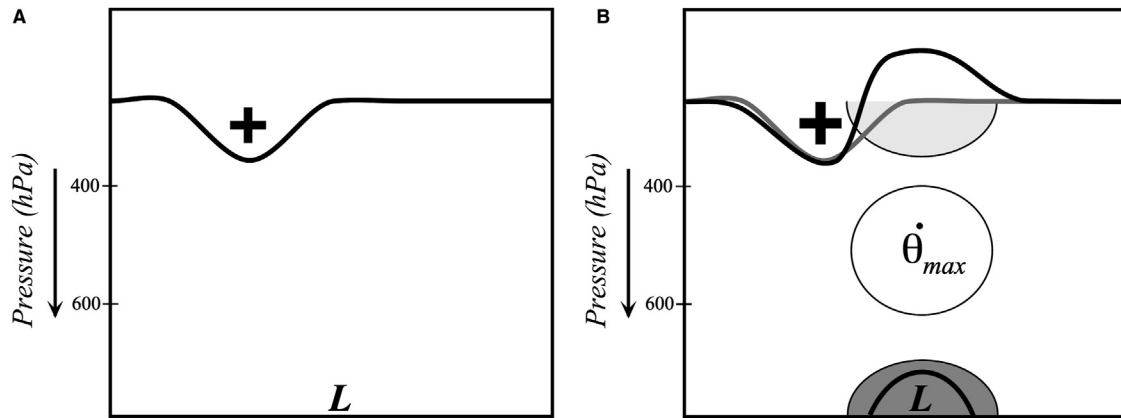
Fig. 26 (A) Relationship between an upper tropospheric positive PV anomaly ("+" sign) and a surface low pressure center ("L"). (B) Ascent downstream of the PV anomaly produces latent heat release manifest as a $\dot{\theta}_{max}$. PV erosion aloft deforms the bold PV contour to the east of the original anomaly, making that anomaly even more anomalous (larger "+" sign). PV production in the lower troposphere intensifies the surface cyclone with high values of PV developing near the center indicated by the bold black line surrounding the "L." Adpated from Martin (2006).

associated cyclonic circulation just like any other positive PV feature and so can contribute to the intensification of the low-level circulation associated with a surface cyclone.

In fact, consideration of the foregoing schematic within the context of a developing cyclone, as in **Fig. 26**, offers a more comprehensive view of the effect of latent heat release on the PV structure. The heating maximum occurs slightly downstream of an upper-level positive PV anomaly since that is where the air is rising most vigorously. As just described, the effects of that heating are to create the low-level positive PV anomaly as well as to erode upper tropospheric PV. This erosion of the upper tropospheric PV serves to steepen the slope of the PV isopleth downstream of the upper-level positive PV anomaly. Such steepening is the PV equivalent of shortening the wavelength between the upper-level trough and the downstream ridge that was emphasized in the description of self-development. From the PV perspective, such an increase in slope also contributes to making the upper PV feature more anomalous. Simultaneously, the cyclonic circulation associated with the low-level positive PV feature enhances both the mutual amplification and phase-locking effects described earlier, leading
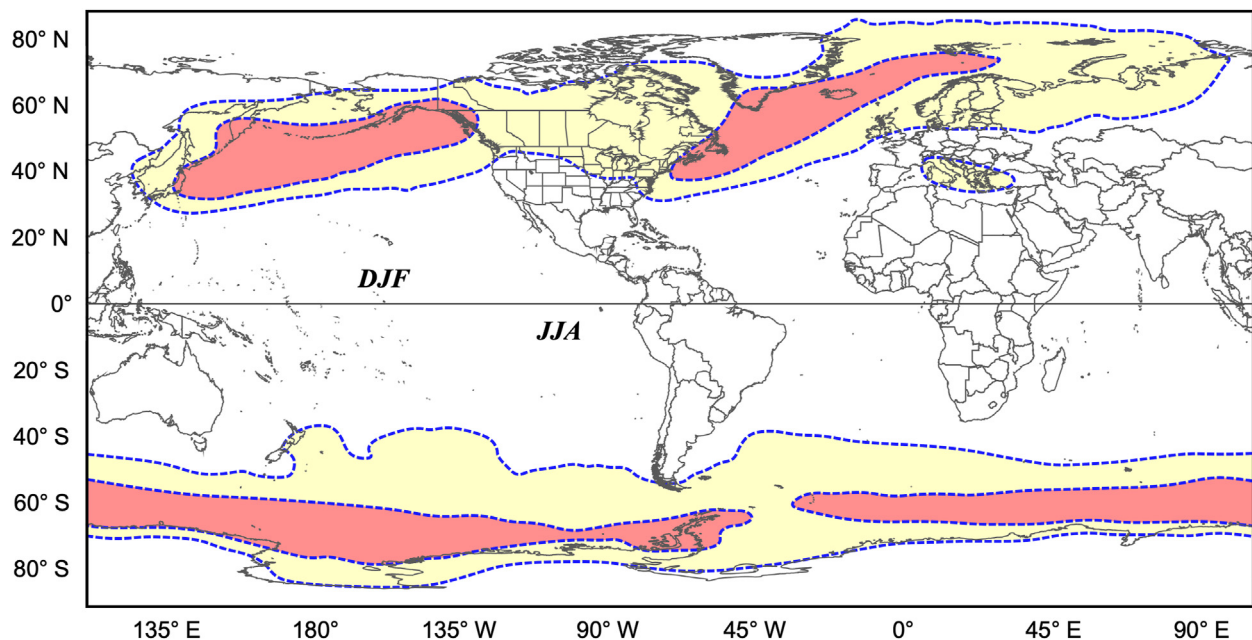
Fig. 27 Wintertime extratropical cyclone track density following the method of Hanley and Caballero (2012). Blue dashed lines are contours of track density in units of 10 tracks $(10^6 \text{ km})^{-1}$ per season with yellow (red) shading indicating 10 (20) tracks $(10^6 \text{ km})^{-1}$ per season. Northern Hemisphere values are for DJF while Southern Hemisphere values are for JJA. Adapted from Shaw et al. (2016).

to continued intensification of the cyclone. Finally, the penetration depth of each anomaly is increased in the presence of latent heating which generally serves to reduce the static stability in such regions.

A Note on the Global Distribution of Extratropical Cyclones

Though extratropical cyclones are observed throughout the middle latitudes, not every location is visited by them with the same regularity. Two predominant storm tracks characterize the Northern Hemisphere winter: the Pacific storm track, extending eastward across the north Pacific Ocean, and the Atlantic storm track, extending northeastward across the north Atlantic Ocean. There is also a slightly less prominent, but separate, track that extends across the Mediterranean Sea and the Middle East known as the Mediterranean storm track. The "track density" of winter extratropical cyclones across the Northern Hemisphere, which clearly identifies these various storm tracks, is shown in the top half of Fig. 27.

A number of physical factors influence the location of these NH storm tracks. One that might seem obvious is that storms are more common along regions of strong sea-surface temperature gradients such as the Kuroshio and Gulf Stream currents. The influence of orography, especially in the lee of the Rocky Mountains in North America, is another substantial factor. The two maxima in track density off the coasts of Asia and North America are related to the outflow of cold continental air over the much warmer ocean in those locations leading to rapid warming of near-surface air and reduction in the static stability which can enhance upward vertical motions.

The wintertime track density in the Southern Hemisphere is quite different (bottom half of Fig. 27). With substantially less land, the asymmetries in diabatic heating that serve to focus extratropical development in the Northern Hemisphere are absent in the SH. Consequently, the distribution is much more zonal with the most frequent tracks located considerably farther poleward. A slight increase in track density appears in the south Atlantic, east of the Andes off the coast of Argentina. The inter-hemispheric differences in winter storm tracks is linked to other dynamical differences in the general circulation characteristics of the hemispheres—a topic that is covered elsewhere in the encyclopedia.

Concluding Statement

This chapter has examined the canonical structure, dynamics and life cycle of extratropical cyclones, the most common large-scale atmospheric disturbance found in the middle latitudes of Earth. The development of these storms, a process known as cyclogenesis, is controlled by large-scale dynamical processes related to the baroclinic westerly shear of the mid-latitudes that itself is an artifact of the pole-to-equator temperature gradient imposed by differential absorption of solar radiation. Specifically, the presence of large-scale waves in this shear promotes differential advection of vorticity in the vertical that, in turn, is associated with low-level convergence and the spin-up of lower tropospheric circulations. This fundamental process is intensified by diabatic feedbacks, most often arising from the release of latent heat associated with the production of precipitation during cyclogenesis. The dynamics of cyclogenesis has been considered from two different but complimentary frameworks; the basic-state variable (omega-centric) and potential vorticity (PV), respectively.

Though not specifically covered in this chapter, the past century's relentless increase in understanding of the extratropical cyclone has contributed to remarkable improvements in operational weather forecasting in the past 50 years —representing, perhaps, one of the most unheralded scientific advances of the second half of the 20th century. Better understanding of the feedbacks between cyclone life cycles and the dynamics of storm tracks and the broader climate system are emerging rapidly and may well shape research on extratropical cyclones for some time to come.

References

Bjerknes, J., Solberg, H., 1922. Life cycle of cyclones and the polar front theory of atmospheric circulation. Geofys. Publ. 3 (1), 1—18.
Charney, J.G., 1947. The dynamics of long waves in a baroclinic westerly current. J. Atmos. Sci. 4, 136—162.
Eady, E.T., 1949. Long waves and cyclone waves. Tellus 1, 33—52.
Hanley, J., Caballero, R., 2012. Objective identification and tracking of multicentre cyclones in the ERA-Interim reanalysis dataset. Q. J. R. Meteorol. Soc. 138, 612—625.
Hoskins, B.J., Draghici, I., Davies, H.C., 1978. A new look at the ω-equation. Q. J. R. Meteorol. Soc. 104, 31—38.
Keyser, D., Reeder, M.J., Reed, R.J., 1988. A generalization of Petterssen's frontogenesis function and its relation to the forcing of vertical motion. Mon. Weather Rev. 116 (3), 762—781.
Martin, J.E., 1999. Quasi-geostrophic forcing of ascent in the occluded sector of cyclones and the trowal airstream. Mon. Weather Rev. 127, 70—88.
Martin, J.E., 2006. Mid-Latitude Atmospheric Dynamics: A First Course. John Wiley and Sons, Chichester, p. 324.
Roebber, P., 1984. Statistical analysis and updated climatology of explosive cyclones. Mon. Weather Rev. 112, 1577—1589.
Sanders, F., Gyakum, J.R., 1980. Synoptic-dynamic climatology of the "bomb". Mon. Weather Rev. 108, 1589—1606.
Shaw, T., Baldwin, M., Barnes, E., et al., 2016. Storm track processes and the opposing influences of climate change. Nat. Geosci. 9, 656—664. https://doi.org/10.1038/ngeo2783.
Sutcliffe, R.C., 1947. A contribution to the problem of development. Q. J. R. Meteorol. Soc. 73, 370—383.
Trenberth, K.E., 1978. On the interpretation of the diagnostic quasi-geostrophic omega equation. Mon. Weather Rev. 106, 131—137.

Further Reading

Crocker, A.M., Godson, W.L., Penner, C.M., 1947. Frontal contour charts. J. Meteorol. 4, 95—99.

Hoskins, B.J., Draghici, I., Davies, H.C., 1978. A new look at the ω-equation. Q. J. R. Meteorol. Soc. 104, 31—38.

Hoskins, B.J., McIntyre, M.E., Robertson, A.W., 1985. On the use and significance of isentropic potential vorticity maps. Q. J. R. Meteorol. Soc. 111, 877—946.

Schultz, D.M., Mass, C.F., 1993. The occlusion process in a midlatitude cyclone over land. Mon. Weather Rev. 121, 918—940.

Sutcliffe, R.C., Forsdyke, A.G., 1950. The theory and use of upper air thickness patterns in forecasting. Q. J. R. Meteorol. Soc. 76, 189—217.

Uccellini, L.W., 1990. Processes contributing to the rapid development of extratropical cyclones. In: Newton, C.W., Holopainen, E.O. (Eds.), Extratropical Cyclones: The Erik Palmen Memorial Volume. Amer. Met. Soc., pp. 81—105.